Marine and Petroleum Geology 25 (2008) 896–905

Contents lists available at ScienceDirect

Marine and Petroleum Geology

journal homepage: www.elsevier.com/locate/marpetgeo

Physical properties of sediments from Keathley Canyon and Atwater Valley, JIP Gulf of Mexico gas hydrate drilling program

William J. Winters [a,*], Brandon Dugan [b], Timothy S. Collett [c]

[a] U.S. Geological Survey, 384 Woods Hole Road, Woods Hole, MA 02543, USA
[b] Rice University, Department of Earth Science, 6100 Main Street, MS-126, Houston, TX 77005, USA
[c] U.S. Geological Survey, Box 25046, MS-939, Denver, CO 80225, USA

ARTICLE INFO

Article history:
Received 14 May 2007
Received in revised form 21 November 2007
Accepted 31 January 2008

Keywords:
Physical properties
Void ratio
Density
Well logging
Gulf of Mexico

ABSTRACT

Physical property measurements and consolidation behavior are different between sediments from Atwater Valley and Keathley Canyon in the northern Gulf of Mexico. Void ratio and bulk density of Atwater Valley sediment from a seafloor mound (holes ATM1 and ATM2) show little effective stress (or depth) dependence to 27 meters below seafloor (mbsf), perhaps owing to fluidized transport through the mound itself with subsequent settling onto the seafloor or mound flanks. Off-mound sediments (hole AT13-2) have bulk physical properties that are similar to mound sediments above 27 mbsf, but void ratio and porosity decrease below that depth. Properties of shallow (<50 mbsf) Keathley Canyon sediments (KC151-3) change with increasing effective stress (or depth) compared to Atwater Valley, but vary little below that depth. Organic carbon is present in concentrations between typical near-shore and deep-sea sediments. Organic carbon-to-nitrogen ratios suggest that the organic matter contained in Atwater Valley off-mound and mound sites came from somewhat different sources. The difference in organic carbon-to-nitrogen ratios between Atwater Valley and Keathley Canyon is more pronounced. At Keathley Canyon a more terrigenous source of the organic matter is indicated. Grain sizes are typically silty clay or clay within the two basins reflecting similar transport energy. However, the range in most shallow sediment properties is significantly different between the two basins. Bulk density profiles agree with logging results in Atwater Valley and Keathley Canyon. Agreement between lab-derived and logging-derived properties supports using logging data to constrain bulk physical properties where cores were not collected.

Published by Elsevier Ltd.

1. Introduction

The properties and behavior of marine sediment are a result of the physical, electrical, and chemical interactions between an extremely complex assemblage of solid grains and fluids. Bulk physical properties, in combination with other measurements, such as grain size, provide not only a means to characterize that sediment, but also can be used to interpret depositional environment and stress history, and to predict shear strength, deformation behavior, and flow properties (e.g., Bowles, 1979; Fang, 1997; Holtz and Kovacs, 1981; Lambe and Whitman, 1969; Mitchell, 1976). Discrete measurements on core samples validate wireline and logging-while-drilling (LWD) data sets, which, in turn, provide high-resolution data for comparisons between different sites or regions. The properties presented here are of interest because relatively few physical property studies have been conducted on gas hydrate bearing sediments in the Gulf of Mexico, particularly sediments near the seafloor (Francisca et al., 2005; Yun et al., 2006).

The northern Gulf of Mexico, which formed from seafloor spreading that occurred during middle Mesozoic time (Bird et al., 2005), has complex deformation and fluid-flow histories that have been influenced by salt tectonics, hydrocarbon generation, rapid sediment accumulation, and erosion. These processes have different effects depending on the location in the Gulf of Mexico and depth below the seafloor. The deep subsurface sediments in the Gulf of Mexico (e.g., Seldon and Flemings, 2005) have been of particular interest due to economic hydrocarbon reserves in the region. In the deepwater Gulf of Mexico, shallow subsurface studies have focused on geohazards and shallow gas accumulations (e.g., Ostermeier et al., 2000). Studies of seeps have characterized leaking gas and gas hydrate within the hydrate stability zone (e.g., MacDonald et al., 2002). Other shallow studies have linked complex interactions between fluid flow, heat transport, and porewater chemistry to explain the distribution of free gas and gas hydrate (e.g., Ruppel et al., 2005).

* Corresponding author: Tel.: +1 508 457 2358.
E-mail address: bwinters@usgs.gov (W.J. Winters).

0264-8172/$ – see front matter Published by Elsevier Ltd.
doi:10.1016/j.marpetgeo.2008.01.018

To provide knowledge about conditions for the occurrence of gas hydrate in the deeper subsurface in the northern Gulf of Mexico, the Chevron Joint Industry Project in 2005 drilled boreholes and recovered core material to depths of several hundreds of meters below the seafloor at sites in the Atwater Valley (AT) and Keathley Canyon (KC) protraction areas (Claypool, 2006). Both sites (Fig. 1) were located in ~1300 m water depth, which ensured common hydrostatic pressure conditions at the seafloor. For studies of sediment properties, the common hydrostatic pressure regime makes it easier to isolate the impact of lithology, porewater chemistry, and consolidation history on the conditions that may govern the occurrence of gas hydrates in the sediments.

In this paper, we use recovered sediment cores to characterize the bulk physical properties of the sediments, to describe how the properties differ at depth and between sites, and to compare the properties with logging data. We determined water content, grain density, and grain size of core samples from Atwater Valley and Keathley Canyon. Wet bulk density and void ratio were determined from mass and volume relations. Consolidation behavior for each drill site was used to describe how deformation varies at the sites. Carbon, hydrogen, and nitrogen contents of select samples were determined because high organic carbon content affects geotechnical properties (Booth and Dahl, 1986), and organic carbon-to-nitrogen ratios provide information about the source of organic matter.

2. Overview

The northern Gulf of Mexico is dominated by salt tectonics, high sedimentation rates, sediment deformation, hydrocarbon generation, and active fluid flow (Coleman and Prior, 1978; Cooper and Hart, 2003; Locat et al., 1996; Prior and Coleman, 1984; Salvador, 1991; Winker and Booth, 2000; Worrall and Snelson, 1989). Deep flow systems in the region are commonly characterized using seismic, logging, and production data (Harrison and Summa, 1991; Flemings and Lupa, 2004; Seldon and Flemings, 2005). Shallow sedimentary systems have been evaluated using seismic data (Hutchinson et al., 2008; Wood et al., 2008), shallow coring activities (Flemings et al., 2006), and seafloor observations (Hart et al., 2008).

The Atwater Valley study area (Fig. 1) is located in Minerals Management Service (MMS) lease blocks 13 and 14 on the floor of the Mississippi Canyon (Hart et al., 2008). Much of the canyon history was influenced by episodes of mass wasting and rapid sedimentation until about 7.5 ka when deposition of hemipelagic clay became dominant (Coleman et al., 1983; Goodwin and Prior, 1989). Regional and local seismic profiles suggest the presence of shallow faults (Cooper and Hart, 2003; Wood et al., 2008) that may be related to local salt diapirism. The faults may provide pathways for fluid migration to the seafloor.

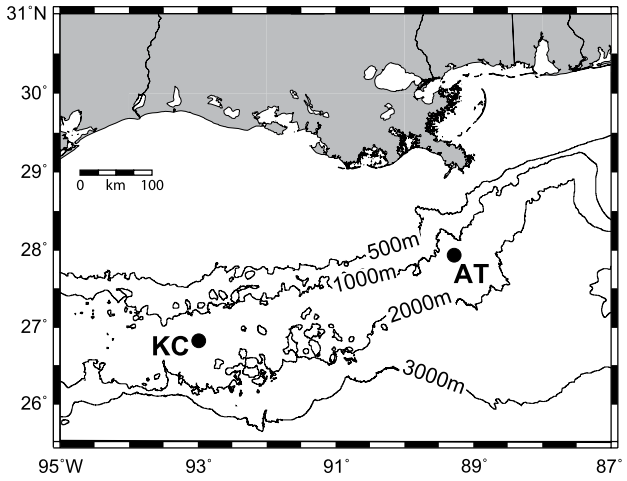

Fig. 1. Base map of the northern Gulf of Mexico locating the Keathley Canyon (KC) and Atwater Valley (AT) study regions. Land is colored grey. Contours are water depth (m).

Hundreds of hydrocarbon seeps exist in the northern Gulf of Mexico (Sager et al., 2003), and numerous mud volcanoes have formed from mobilized sediment of various ages ejected onto the seafloor due to overpressure (Kohl and Roberts, 1995; Roberts, 2001; Sager et al., 2003). Sager et al. (2003) describe a number of acoustic features indicative of different mound formation mechanisms and evolution; however, they note that direct physical property measurements are necessary to confirm geophysical interpretations. A number of sediment mounds are present on the seafloor at Atwater Valley (Hart et al., 2008). Sites were drilled to document sediment and fluid properties on an active mound (ATM1, ATM2) and its surrounding region (AT13-1, AT13-2). The ATM1 and ATM2 drill sites are located on "Mound F", which is a few hundred meters in diameter and ~10 m high, and has a feature caused by a mud flow on the southeastern flank (Hart et al., 2008). Elevated heat flow values (Coffin et al., 2008) and porewater salinity (Table 1) (Kastner et al., 2008) in the vicinity or on the mounds support the interpretation of mound building due to fluid flow from depth.

AT13-1 (27.9471°N, 89.2893°W, water depth: 1290.5 m) and AT13-2 (27.9471°N, 89.2893°W, water depth: 1291.1 m) are twinned holes located between two seafloor mounds. AT13-1 was a logging-while-drilling (LWD) hole, and AT13-2 was used for coring. Coring was conducted at ATM1 (27.9366°N, 89.2795°W, water depth: 1296.0 m) and ATM2 (27.9366°N, 89.2797°W, water depth: 1295.4 m).

The Keathley Canyon sites are located in MMS lease block 151 about 387 km west of Atwater Valley (Fig. 1) along an intraslope, salt-withdrawal mini-basin (Casey basin) with faults and seafloor vents nearby. The stratigraphic architecture of the upper 400 m of the southeastern edge of this basin consists of seven seismic units in three groups as described by Hutchinson et al. (2008). Sediment near the seafloor (0 to about 75 mbsf) consists of modern hemipelagic drape. The intermediate strata (~75–160 mbsf) in the well consist of fine-grained deposits with several sand or sand-rich layers up to 15 m thick between 95 mbsf and 150 mbsf (Collett, 2006), and the lower section (about 160–375 mbsf) consists of fine-grained muds (Hutchinson et al., 2008). Two depth intervals (220–230 mbsf and 264–298 mbsf) are believed to contain gas hydrate deposits possibly within near-vertical fractures (Lee and Collett, 2008; Hutchinson et al., 2008).

KC151-2 (LWD) (26.8230°N, 92.9865°W, water depth: 1321.9 m) and KC151-3 (coring) (26.8230°N, 92.9867°W, water depth: 1322.5 m) are twinned holes that provide petrophysical and bulk physical properties of sediments recovered on the flank of the mini-basin.

3. Methods

Standard, non-pressurized cores were collected using either a Fugro Hydraulic Piston Corer (FHPC) or a Fugro Corer (FC) (Claypool, 2006; Fugro-McClelland Marine Geosciences, Inc., 2006). Adjacent subsamples from cores were collected for bulk physical property analysis (Table 1) and for grain-size analysis (Table 2). We calculated physical properties on small specimens ($<10\ cm^3$) and assumed 100% water saturation. This allowed the physical property measurements to approximate in situ conditions without being adversely influenced by coring disturbance and expansion voids.

Table 1
Physical properties of sediment from AT13-2, ATM1, ATM2, and KC151-3

Depth (mbsf)	Salinity (ppt)	Water content (solids) (%)	Grain density (kg m^{-3})	Bulk density (kg m^{-3})	Void ratio
Hole: AT13-2					
3	34.0	69.7	2687	1614	1.82
6.3	32.9	63.7	2689	1648	1.67
8.31	32.4	64.5	2690	1643	1.69
10.01	32.0	65.0	2683	1638	1.70
12.35	32.0	62.1	2681	1655	1.63
14.65	32.0	60.2	2682	1668	1.58
19.59	32.0	63.4	2683	1648	1.66
21.79	32.0	59.4	2690	1675	1.56
23.59	32.3	69.4	2680	1613	1.82
25.29	32.6	66.0	2717	1640	1.75
29.95	33.5	62.7	2701	1657	1.65
32.65	33.5	34.6	2689	1898	0.91
36.74	34.9	57.2	2704	1696	1.51
41.11	36.4	54.6	2699	1715	1.43
42.92	37.0	51.6	2696	1737	1.35
44.99	36.9	65.4	2697	1642	1.72
47.82	36.7	54.2	2702	1719	1.42
119.26	31.6	47.7	2704	1768	1.26
120.56	31.5	40.6	2698	1832	1.07
122.46	31.3	43.6	2692	1802	1.15
123.52	31.2	50.6	2701	1742	1.33
128.8	30.9	49.4	2695	1750	1.30
131.8	31.2	49.1	2689	1751	1.29
142.8	32.5	57.9	2693	1686	1.52
143.32	32.5	53.6	2690	1717	1.41
147.65	32.5	56.8	2688	1693	1.49
149.5	32.5	58.9	2697	1680	1.55
158.33	33.0	49.2	2701	1754	1.30
Minimum	30.9	34.6	2680	1613	0.91
Maximum	37.0	69.7	2717	1898	1.82
Range	6.1	35.0	37	285	0.92
Mean	33.0	56.5	2694	1703	1.48
Median	32.5	57.6	2692	1690	1.51
Standard deviation	1.8	8.7	9	68	0.23
Hole: ATM1					
0.78	56.0	73.6	2704	1614	1.91
2.21	55.7	65.5	2703	1658	1.70
8.57	54.1	72.3	2701	1619	1.87
10.46	52.6	71.3	2705	1624	1.85
11.47	51.9	68.1	2703	1640	1.77
13.52	52.0	69.8	2703	1631	1.82
14.32	53.2	62.9	2703	1672	1.63
14.97	54.2	62.3	2704	1677	1.62
16.37	55.2	67.3	2706	1648	1.75
20.65	56.0	72.7	2707	1619	1.89
22.75	56.0	70.0	2706	1633	1.82
24.9	55.5	64.6	2707	1664	1.68
26.95	55.0	61.5	2703	1682	1.59
Minimum	51.9	61.5	2701	1614	1.59
Maximum	56.0	73.6	2707	1682	1.91
Range	4.1	12.1	6	68	0.31
Mean	54.4	67.8	2704	1645	1.76
Median	55.0	68.1	2704	1640	1.77
Standard deviation	1.5	4.2	2	24	0.11
Hole: ATM2					
1	55.5	66.3	2707	1654	1.72
2.5	55.5	69.6	2701	1634	1.80
9.92	55.1	63.6	2702	1669	1.65
12.32	55.0	71.1	2692	1624	1.84
13.47	54.9	64.6	2692	1660	1.67
18.37	53.8	66.0	2701	1653	1.71
20.37	53.3	64.8	2703	1660	1.68
20.87	53.3	64.0	2701	1665	1.66
22.87	53.8	62.1	2699	1676	1.61
26.32	54.0	64.4	2700	1663	1.67
Minimum	53.3	62.1	2692	1624	1.61
Maximum	55.5	71.1	2707	1676	1.84
Range	2.2	9.0	15	53	0.23
Mean	54.4	65.6	2700	1656	1.70
Median	54.5	64.7	2701	1660	1.68
Standard deviation	0.9	2.8	5	16	0.07
Hole: KC151-3					
2.5	35.0	79.2	2736	1576	2.11
4.25	35.0	100.7	2736	1491	2.69
6.7	35.4	90.7	2721	1525	2.40
9.95	37.7	78.0	2670	1572	2.02
12.95	39.3	54.2	2704	1721	1.42
13.95	39.8	62.6	2695	1661	1.64
16.2	40.5	59.0	2702	1687	1.55
19.08	42.2	55.9	2706	1711	1.47
20.84	43.5	54.4	2705	1723	1.42
24.34	44.4	54.4	2729	1730	1.44
28.49	44.5	49.1	2725	1771	1.29
30.99	44.7	45.2	2730	1807	1.19
34.24	45.0	48.0	2722	1781	1.26
39.54	45.0	39.5	2724	1862	1.04
41.79	45.0	45.4	2722	1803	1.19
43.54	44.9	39.2	2722	1864	1.03
102.57	36.1	37.8	2718	1872	1.00
215.63	49.4	34.3	2690	1912	0.89
217.23	49.8	37.0	2738	1899	0.97
223.61	50.0	32.7	2721	1944	0.86
225.36	50.1	31.0	2721	1966	0.81
230.62	50.9	34.5	2718	1922	0.90
242.26	50.1	36.4	2739	1906	0.96
244.51	50.6	35.6	2744	1917	0.94
252.57	51.9	34.6	2732	1926	0.91
253.82	52.0	37.2	2732	1896	0.98
257.53	52.4	38.9	2744	1881	1.03
259.33	51.6	46.9	2739	1800	1.23
261.38	51.0	31.0	2730	1971	0.81
275.32	51.0	40.2	2695	1850	1.04
276.82	50.9	36.3	2675	1884	0.94
279.12	50.3	34.6	2671	1903	0.89
281.32	50.1	35.5	2672	1893	0.91
294.41	51.9	35.1	2719	1916	0.92
297.41	53.0	35.7	2725	1911	0.94
300.16	53.6	34.3	2717	1926	0.89
312.06	54.0	34.2	2734	1933	0.90
313.66	53.7	29.4	2726	1993	0.77
330.8	50.3	37.7	2742	1892	0.99
333	50.1	34.3	2725	1926	0.90
369.67	54.9	34.8	2747	1931	0.92
371.52	54.9	39.7	2746	1875	1.05
378.78	54.1	32.0	2734	1961	0.84
Minimum	35.0	29.4	2670	1491	0.77
Maximum	54.9	100.7	2747	1993	2.69
Range	19.9	71.3	77	502	1.92
Mean	47.5	44.6	2719	1835	1.17
Median	50.1	37.7	2724	1884	0.99
Standard deviation	5.9	16.3	21	126	0.43

The dried physical property samples were also used to determine carbon, hydrogen, and nitrogen contents (Table 3).

3.1. Bulk physical properties

Moisture and density (MAD) analyses provide bulk physical properties of sediment samples (Blum, 1997). All mass measurements were made quickly using sealed containers to prevent moisture from being adsorbed by clay minerals. The mass of a wet sediment sample (M_t) was recorded and then the sample was oven dried at 110 °C for at least 24 h (American Society for Testing and Materials, 2006). The mass of evaporated water defines the mass of fresh water (M_{fw}) in the specimen. The mass of salt (M_{salt}) in each specimen is determined from the salinity (S) in parts per thousand (ppt) according to $M_{salt} = M_{fw}(S/(1000 - S))$. Salinity was interpolated from shipboard porewater measurements of cored

Table 2
Extrapolated grain-size results determined with a Coulter Counter

Depth (mbsf)	Sediment classification	% Sand	% Silt	% Clay size	D_{60} (μm)	D_{50} (μm)	D_{10} (μm)	C_U	Skewness	Kurtosis
Hole: AT13-2										
5.00	Silty clay	2.30	27.92	69.78	2.40	1.72	0.47	5.14	−0.35	0.27
8.31	Clay	1.01	22.85	76.13	2.17	1.68	0.49	4.40	−0.37	0.84
10.01	Clay	1.39	21.93	76.68	1.80	1.45	0.46	3.91	−0.40	0.85
12.35	Silty clay	1.65	23.92	74.43	1.95	1.63	0.56	3.49	−0.42	0.90
14.65	Clay	1.12	16.48	82.40	2.15	1.75	0.64	3.37	−0.48	2.41
19.59	Clay	0.54	17.60	81.86	1.69	1.39	0.46	3.67	−0.42	1.50
21.79	Clay	0.58	20.16	79.27	1.82	1.54	0.54	3.36	−0.38	0.97
23.59	Clay	0.22	16.89	82.89	1.72	1.46	0.52	3.32	−0.35	1.45
25.29	Clay	0.54	18.78	80.68	1.72	1.41	0.47	3.65	−0.35	0.81
29.95	Silty clay	0.33	28.94	70.73	2.21	1.64	0.51	4.36	−0.27	−0.19
32.65	Silty clay	0.69	24.60	74.71	1.89	1.51	0.48	3.91	−0.33	0.37
36.74	Silty clay	1.03	24.17	74.80	1.83	1.42	0.42	4.33	−0.36	0.27
41.11	Clay	2.96	20.07	76.97	1.82	1.53	0.53	3.45	−0.53	1.33
42.92	Clay	0.56	20.57	78.87	1.77	1.45	0.49	3.61	−0.38	0.93
44.99	Clay	0.33	16.55	83.12	1.63	1.36	0.47	3.46	−0.35	1.40
47.82	Silty clay	3.38	22.16	74.46	1.91	1.50	0.46	4.14	−0.45	0.79
119.26	Silty clay	3.37	24.74	71.89	2.05	1.60	0.51	4.03	−0.44	0.43
120.56	Silty clay	1.87	25.42	72.71	2.03	1.58	0.49	4.11	−0.39	0.48
122.46	Clay	3.22	20.57	76.21	1.76	1.47	0.51	3.44	−0.54	1.54
123.52	Clay	0.15	20.07	79.78	1.70	1.36	0.42	4.08	−0.29	0.34
128.80	Silty clay	1.50	24.40	74.10	1.89	1.53	0.50	3.80	−0.41	0.55
131.80	Silty clay	6.47	31.86	61.67	3.46	1.85	0.51	6.73	−0.26	−0.86
142.80	Silty clay	2.09	33.25	64.66	2.92	1.76	0.48	6.04	−0.25	−0.74
143.32	Clay	1.99	21.23	76.78	1.74	1.37	0.41	4.28	−0.45	0.76
147.65	Silty clay	0.30	25.76	73.94	1.86	1.68	0.43	4.33	−0.32	−0.04
149.50	Clay	0.85	14.32	84.83	1.70	1.36	0.42	4.03	−0.63	5.21
158.33	Clay	0.76	21.72	77.53	1.76	1.38	0.42	4.23	−0.38	0.58
Minimum		0.15	14.32	61.67	1.63	1.36	0.41	3.32	−0.63	−0.86
Maximum		6.47	33.25	84.83	3.46	1.85	0.64	6.73	−0.25	5.21
Range		6.32	18.93	23.16	1.84	0.49	0.23	3.40	0.38	6.07
Mean		1.53	22.48	76.00	1.98	1.53	0.48	4.10	−0.39	0.86
Median		1.03	21.93	76.21	1.83	1.51	0.48	4.03	−0.38	0.79
Standard deviation		1.41	4.58	5.39	0.40	0.14	0.05	0.79	0.09	1.11
Hole: ATM1										
0.78	Silty clay	2.04	33.29	64.67	2.94	1.78	0.49	5.99	−0.23	−0.40
2.21	Silty clay	1.77	24.51	73.73	1.83	1.50	0.48	3.80	−0.40	0.44
8.57	Silty clay	2.14	27.40	70.46	2.32	1.65	0.46	5.02	−0.33	0.28
10.46	Silty clay	2.07	29.42	68.51	2.46	1.65	0.45	5.43	−0.31	0.00
11.47	Silty clay	2.07	23.79	74.15	1.91	1.48	0.43	4.42	−0.41	0.71
13.52	Silty clay	2.01	25.86	72.13	2.04	1.51	0.42	4.83	−0.37	0.44
14.32	Silty clay	2.07	26.91	71.02	2.11	1.54	0.44	4.82	−0.36	0.18
14.97	Silty clay	2.27	26.26	71.47	2.06	1.48	0.41	5.07	−0.37	0.19
16.37	Silty clay	2.20	32.44	65.36	2.96	1.84	0.47	6.35	−0.28	−0.28
20.65	Silty clay	3.79	28.91	67.31	2.62	1.69	0.45	5.77	−0.38	0.30
22.75	Silty clay	1.96	24.00	74.04	1.95	1.50	0.44	4.44	−0.40	0.53
24.90	Silty clay	1.98	24.75	73.27	2.03	1.52	0.43	4.70	−0.37	0.70
26.95	Silty clay	2.82	27.63	69.55	2.41	1.66	0.47	5.07	−0.36	0.37
Minimum		1.77	23.79	64.67	1.83	1.48	0.41	3.80	−0.41	−0.40
Maximum		3.79	33.29	74.15	2.96	1.84	0.49	6.35	−0.23	0.71
Range		2.02	9.50	9.48	1.13	0.36	0.09	2.56	0.18	1.11
Mean		2.25	27.32	70.44	2.28	1.60	0.45	5.06	−0.35	0.27
Median		2.07	26.91	71.02	2.11	1.54	0.45	5.02	−0.37	0.30
Standard deviation		0.59	5.21	3.20	0.38	0.12	0.02	0.70	0.05	0.34
Hole: ATM2										
1.00	Silty clay	2.66	33.58	63.76	3.10	1.84	0.53	5.83	−0.27	−0.34
2.50	Silty clay	2.45	34.39	63.15	3.36	2.08	0.51	6.63	−0.22	−0.30
9.92	Clay	1.94	21.46	76.60	1.74	1.32	0.38	4.56	−0.45	0.84
12.32	Clay	2.16	7.61	90.23	1.28	1.02	0.33	3.89	−0.82	4.57
13.47	Silty clay	2.29	33.69	64.02	3.16	1.90	0.51	6.19	−0.26	−0.20
18.37	Clay	2.13	20.02	77.85	1.74	1.39	0.43	4.06	−0.48	1.35
20.37	Silty clay	2.84	39.04	58.12	3.95	2.41	0.50	7.94	−0.18	−0.79
20.87	Silty clay	3.48	26.01	70.51	2.44	1.67	0.45	5.46	−0.40	0.36
22.87	Silty clay	2.47	26.84	70.69	2.16	1.52	0.41	5.24	−0.38	0.19
26.32	Silty clay	3.42[a]	25.24	71.34	2.02	1.47	0.41	4.95	−0.76	3.78
Minimum		1.94	7.61	58.12	1.28	1.02	0.33	3.89	−0.82	−0.79
Maximum		3.48	39.04	90.23	3.95	2.41	0.53	7.94	−0.18	4.57
Range		1.54	31.43	32.11	2.66	1.39	0.20	4.06	0.64	5.36
Mean		2.49	26.79	70.63	2.50	1.66	0.45	5.48	−0.42	0.95
Median		2.45	26.43	70.60	2.30	1.60	0.44	5.35	−0.39	0.28
Standard deviation		0.46	9.11	9.28	0.86	0.40	0.07	1.24	0.22	1.82

(*continued on next page*)

Table 2 (*continued*)

Depth (mbsf)	Sediment classification	% Sand	% Silt	% Clay size	D_{60} (μm)	D_{50} (μm)	D_{10} (μm)	C_U	Skewness	Kurtosis
Hole: KC151-3										
2.50	Clay	0.52	23.44	76.04	2.00	1.60	0.51	3.93	−0.23	0.72
4.25	Clay	2.17	10.01	87.82	1.67	1.44	0.53	3.13	−0.86	6.02
6.70	Clay	1.56	9.01	89.43	1.65	1.44	0.53	3.11	−0.83	6.79
9.95	Clay	0.21	16.01	83.78	1.75	1.49	0.53	3.29	−0.37	1.81
12.95	Silty clay	0.04	42.74	57.22	4.68	2.81	0.78	6.00	−0.03	−0.89
13.95	Silty clay	0.05	31.44	68.52	3.07	2.32	0.80	3.82	−0.20	−0.23
16.20	Silty clay	0.03	30.38	69.60	2.65	1.86	0.61	4.37	−0.19	−0.22
19.08	Silty clay	0.05	32.85	67.09	3.35	1.83	0.52	6.45	−0.14	−0.56
20.84	Silty clay	0.04	43.35	56.60	4.61	2.79	0.53	8.68	0.02	−0.98
24.34	Silty clay	0.03	27.35	72.62	2.25	1.66	0.50	4.47	−0.12	−0.33
28.49	Silty clay	0.05	34.97	64.98	3.07	1.92	0.51	6.01	−0.02	−0.84
30.99	Silty clay	0.02	32.33	67.66	2.78	1.85	0.51	5.44	−0.05	−0.70
34.24	Silty clay	0.05	25.46	74.49	2.21	1.64	0.49	4.52	−0.08	−0.35
39.54	Silty clay	0.05	33.22	66.73	2.89	1.88	0.50	5.83	−0.09	−0.50
41.79	Clay	0.13	19.51	80.36	1.81	1.43	0.44	4.16	−0.16	0.23
43.54	Silty clay	0.05	31.81	68.14	2.93	2.06	0.52	5.61	0.01	−0.51
102.47	Clayey silt	0.10	57.11	42.79	15.99	6.91	0.63	25.52	0.13	−1.29
215.63	Silty clay	0.66	30.69	68.65	2.58	1.72	0.41	6.29	−0.22	−0.24
217.23	Clay	0.25	15.71	84.04	1.66	1.33	0.41	4.05	−0.47	1.36
223.61	Silty clay	0.30	27.20	72.49	2.32	1.64	0.45	5.09	−0.12	−0.22
225.36	Silty clay	0.94	32.51	66.55	3.00	2.01	0.51	5.83	−0.20	0.11
230.62	Silty clay	1.45	26.48	72.07	2.30	1.64	0.46	5.00	−0.31	0.64
242.62	Silty clay	0.11	28.64	71.25	2.45	1.72	0.49	5.02	−0.09	−0.39
244.51	Clay	0.07	22.06	77.87	1.97	1.51	0.44	4.53	−0.08	−0.29
252.57	Silty clay	0.06	31.07	68.87	2.72	1.86	0.51	5.36	−0.07	−0.38
253.82	Silty clay	0.08	35.43	64.49	3.23	2.11	0.50	6.41	−0.04	−0.68
257.53	Clay	1.05	15.51	83.44	1.74	1.35	0.41	4.23	−0.53	3.49
259.33	Clay	2.55	8.83	88.62	1.53	1.30	0.44	3.45	−0.90	5.31
261.38	Clay	0.15	20.07	79.77	1.81	1.42	0.43	4.24	−0.14	0.21
275.32	Clay	0.07	20.17	79.75	1.78	1.45	0.48	3.73	−0.24	0.31
276.82	Clay	0.02	15.82	84.17	1.69	1.43	0.50	3.35	−0.16	0.58
279.12	Clay	0.01	16.96	83.03	1.71	1.45	0.51	3.34	−0.20	0.57
294.41	Clay	0.03	18.22	81.75	1.76	1.47	0.51	3.45	−0.22	0.46
297.41	Clay	0.03	17.36	82.61	1.78	1.51	0.54	3.28	−0.26	1.02
300.16	Clay	0.03	22.54	77.43	1.81	1.49	0.50	3.65	−0.17	−0.23
312.06	Silty clay	0.08	31.25	68.67	2.60	1.74	0.48	5.38	−0.08	−0.68
313.66	Silty clay	0.03	28.88	71.08	2.30	1.67	0.50	4.59	−0.08	−0.63
330.80	Silty clay	0.08	31.65	68.26	2.73	1.83	0.51	5.39	−0.09	−0.49
333.00	Silty clay	0.04	30.74	69.23	2.60	1.80	0.55	4.76	−0.07	−0.51
369.67	Clay	0.27	7.15	92.58	1.68	1.48	0.53	3.18	−0.37	6.98
371.52	Clay	0.29	13.49	86.22	1.82	1.56	0.58	3.12	−0.45	4.32
378.78	Silty clay	0.06	28.56	71.38	2.41	1.73	0.52	4.66	−0.11	−0.34
Minimum		0.01	7.15	42.79	1.53	1.30	0.41	3.11	−0.90	−1.29
Maximum		2.55	57.11	92.58	15.99	6.91	0.80	25.52	0.13	6.98
Range		2.54	49.96	49.79	14.46	5.61	0.39	22.41	1.03	8.27
Mean		0.33	25.67	74.00	2.68	1.83	0.51	5.09	−0.21	0.67
Median		0.07	27.28	72.28	2.30	1.64	0.51	4.52	−0.16	−0.23
Standard deviation		0.59	10.20	9.95	2.20	0.86	0.08	3.41	0.22	2.11

[a] Includes 1.11% gravel.

materials (Kastner et al., 2006) (Table 1). The mass of solid grains (M_s) was determined from M_t, M_{salt}, and M_{fw} using $M_s = M_t - M_{fw} - M_{salt}$.

Each oven dried specimen was placed in a 10 cm^3 cup, and the volume of dry solids (V_s) was determined with an automatic gas pycnometer using helium as the purge and expansion gas (American Society for Testing and Materials, 1997). Volume of dry solids was corrected to remove the volume of salt. Grain density (ρ_s) was then calculated from $\rho_s = M_s/V_s$.

The total volume of each specimen ($V_t = V_s + V_{sw}$) was determined assuming 100% water saturation. The volume of seawater (V_{sw}) was determined from the seawater density (ρ_{sw}): $V_{sw} = (M_{fw} + M_{salt})/\rho_{sw}$, where ρ_{sw} [kg m^{-3}] = 999.78 + 770 (S/1000), which is modified from Couper (1983). Seawater density values incorporating salinity, temperature, and pressure can be obtained from other sources (e.g., Brydon et al., 1999; Wright, 1997). These measurements and calculations are used to define wet bulk density ($\rho_b = M_t/V_t$), void ratio ($e = V_{sw}/V_s$), and solid mass-based water content (WC = M_{sw}/M_s).

3.2. Grain size

Grain-size analyses were performed on specimens adjacent to those used for MAD analyses. Each grain-size specimen was oven dried at 90 °C to determine component masses and water content. Similar to MAD analyses, dry mass was corrected for salt.

Each specimen was then wet-sieved using distilled water through a number 230 sieve (0.062-mm mesh) to separate the coarse (>0.062 mm) and fine (<0.062 mm) fractions. The suspension containing the fine fraction was sonicated for 30 s to disaggregate the sample and then stirred to homogenize it. A split of the sample was removed and placed into a 4% NaCl solution to obtain the proper concentration in the suspension. The fine fraction distribution was measured with a Coulter Counter electro-resistance multi-channel particle-size analyzer using time of transition theory (Syvitski, 1991). The Coulter Counter is calibrated to 0.6 μm, and sediment below that size is not measured. To help overcome that limitation, the grain-size results were extrapolated to 0.12 μm (Poppe et al., 2004). Using that method, the slope of the original

Table 3
Carbon, hydrogen, and nitrogen (CHN) results

Depth (mbsf)	Organic carbon (OC) (%)	Inorganic carbon (IC) (%)	Hydrogen (average) (%)	Total nitrogen (TN) (average) (%)	OC/TN
Hole: AT13-2					
6.30	0.74	0.53	0.61	0.08	9.25
14.65	0.70	0.54	0.62	0.08	8.75
25.29	0.67	0.55	0.61	0.09	7.44
42.92	0.62	0.56	0.58	0.08	7.75
122.46	0.65	0.57	0.52	0.07	9.29
143.32	0.62	0.66	0.55	0.07	8.86
Minimum	0.62	0.53	0.52	0.07	7.44
Maximum	0.74	0.66	0.62	0.09	9.29
Range	0.12	0.13	0.10	0.02	1.84
Mean	0.67	0.57	0.58	0.08	8.56
Median	0.66	0.56	0.59	0.08	8.80
Standard deviation	0.05	0.05	0.04	0.01	0.78
Hole: ATM1					
2.21	0.58	1.33	0.53	0.06	9.67
13.52	0.59	1.44	0.55	0.06	9.83
20.65	0.61	1.31	0.58	0.06	10.17
26.95	0.57	1.33	0.51	0.06	9.50
Minimum	0.57	1.31	0.51	0.06	9.50
Maximum	0.61	1.44	0.58	0.06	10.17
Range	0.04	0.13	0.07	0.01	0.67
Mean	0.59	1.35	0.54	0.06	9.79
Median	0.59	1.33	0.54	0.06	9.75
Standard deviation	0.02	0.06	0.03	0.00	0.28
Hole: KC151-3					
4.25	0.48	2.65	0.80	0.05	9.60
13.95	0.82	1.58	0.59	0.05	16.40
24.34	0.95	1.93	0.71	0.07	13.57
41.79	0.77	1.45	0.70	0.07	11.00
102.57	0.44	1.16	0.49	0.05	8.80
217.23	0.68	2.48	0.79	0.05	13.60
275.32	0.95	1.17	0.77	0.07	13.57
300.16	0.88	1.11	0.74	0.08	11.00
Minimum	0.44	1.11	0.49	0.05	8.80
Maximum	0.95	2.65	0.80	0.08	16.40
Range	0.51	1.54	0.31	0.04	7.60
Mean	0.75	1.69	0.70	0.06	12.19
Median	0.80	1.52	0.72	0.06	12.29
Standard deviation	0.20	0.60	0.11	0.01	2.52

distribution curve greater than 0.6 μm was used to define an extrapolated slope smaller than 0.6 μm. The resultant distribution curve was then used to determine parameters representative of a finer-sized sediment. Results were not corrected for mineralogical surface conduction effects, as these have not been raised as an issue with Coulter Counter analyses (Poppe et al., 2005; Syvitski, 1991). Hydrocarbons were not visually observed in any of the grain-size samples.

The percent of sand, silt, and clay size grains in the samples is based on the grade scale of Wentworth (1929) and classification scheme of Shepard (1954). The median sediment diameter (D_{50}), and diameters at which 60% (D_{60}) and 10% (D_{10}) of the entire dry mass of the sediment are finer were determined from a cumulative-frequency curve constructed for each sample. These data were used to evaluate the uniformity coefficient C_u, given by D_{60}/D_{10}. The method of moments was used to determine skewness and kurtosis, two additional measures of grain-size sorting (Boggs, 1992). Skewness is related to the distribution of particles on each side of a grain-size frequency curve, whereas kurtosis is a measure of the steepness in the central portion of the curve. Details of the grain size procedure are provided by Poppe et al. (2005).

3.3. Carbon, hydrogen, and nitrogen (CHN) contents

CHN contents of dried sediment were determined with a Perkin Elmer 2400 series II Carbon–Hydrogen–Nitrogen–Sulphur–Oxygen Analyzer which used a combustion method to convert sample elements to simple gases such as CO_2, H_2O, and N_2 (Jablonski et al., 2002; Verardo et al., 1990). The resulting gases were homogenized, depressurized, and quantified as a function of their thermal conductivities.

Two dried samples were tested for each reported depth. Total carbon (TC) was measured on the first sample. Before testing the second sample, it was acidified to remove all inorganic carbonate matter by the addition of sulfurous acid. Using this method, only the organic carbon (OC) was further analyzed. The inorganic carbon (IC) is assumed to be the difference between TC and OC.

4. Results and discussion

Sediment properties are influenced by a host of factors including texture, particle shape, mineralogy, rate of deposition, porewater chemistry, consolidation due to physical processes, and diagenesis. During burial with normal consolidation, pore fluids escape as the overburden stress increases. This results in a time-dependent loss of pore volume which decreases water content and void ratio, and increases bulk density. The Atwater Valley mound and off-mound sites have similar water contents (~75–60%) to 27 mbsf (Fig. 2) that vary much less than at KC151-3. Water content in Keathley Canyon decreases from ~100% to 30% from the seafloor to 379 mbsf (Fig. 2) (Table 1). These results are in general agreement with values from the same holes reported by Yun et al. (2006) in a study that also included shear strength, acoustic velocity, and other index properties. We have complemented and expanded that work by interpreting geologic influences on measurements, grain-size analyses, and CHN analyses. Our results are also in overall agreement with a post-cruise report on geotechnical properties produced by Fugro-McClelland Marine Geosciences, Inc. (2006).

Drying temperature is assumed to have little effect on the water content and related properties (e.g., Winters, 2000). However, no mineralogical studies have been conducted on these samples to rule out the presence of montmorillonite, a clay mineral that is highly influenced by oven drying (Lambe, 1951). Scanning electron microscopy and specific surface measurements suggest that illite and some montmorillonite may be present (Yun et al., 2006), although illite probably dominates. Francisca et al. (2005) also determined specific surface for near-seafloor (<3.5 mbsf) sediments at three locations in the northern Gulf of Mexico. Those samples, including nine from or near a 1.5-km-wide and 30-m high, normally consolidated mud volcano in the Mississippi Canyon also supported illite as the dominant clay mineral. Lambe (1951) reported the effect of oven drying on five widely different soils, one of which was Boston blue clay, an illitic marine clay that exhibited less than 0.5% water content change over a temperature variation from about 80 °C to 190 °C. Since Boston blue clay has a lower plasticity (Cerato and Lutenegger, 2004) than the JIP drill sites (Yun et al., 2006), more than a 0.5% increase in water content would occur in the JIP samples over the same temperature range. However, the higher plasticity of the JIP samples is offset by a lower drying temperature. Therefore, drying temperature is not expected to significantly affect the water content of the JIP sediment.

Void ratio decreases with increasing depth in a manner similar to water content (Fig. 2). The largest decrease in void ratio, 2.7–0.77, occurs at KC151-3 (Fig. 3B) (Table 1). Void ratios at AT13-2 also decrease with depth, but the decrease, especially above 27 mbsf is less pronounced (Fig. 3A) (Table 1). We use a void ratio–effective vertical stress (e–σ_v') model to define the consolidation behavior at each site (Lambe and Whitman, 1969): $e = e_o - C_c \log \sigma_v'$, where e_o

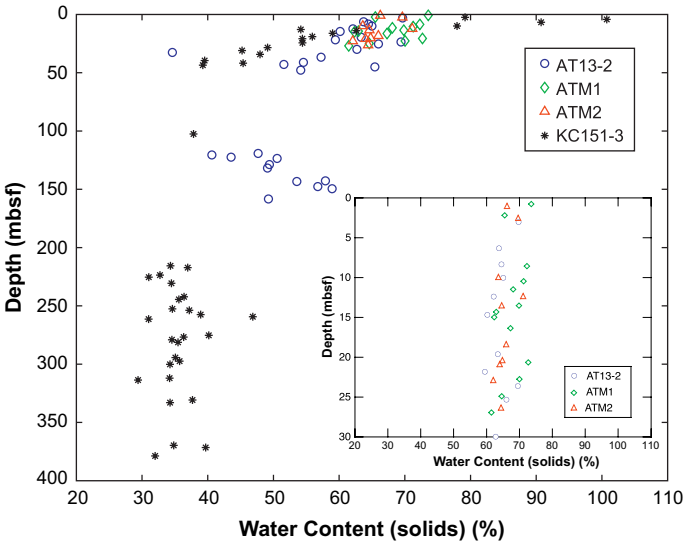

Fig. 2. Solid mass-based water contents (WC) from the four coring sites (AT13-2, ATM1, ATM2, KC151-3) used in this study. WC at KC151-3 has high variability in the shallow subsurface, decreases with depth, and has less variability below 200 mbsf. Insert shows uniformity of water content in the upper 30 m at Atwater Valley.

is the void ratio at a reference vertical effective stress (1 kPa). C_c is the compression index. Vertical effective stress is calculated by integrating the bulk density data minus an average seawater density of 1024 kg m^{-3}. Model parameters were constrained through regressions on data above 50 mbsf assuming fluid pressure is hydrostatic. This allows comparison between shallow and deep data at AT13-2 and KC151-3.

AT13-2 has a compression index of 0.31 and a reference void ratio of 2.22. These parameters define the best-fit model to the shallow data (<50 mbsf) and also provide a reasonable fit to the void ratio observations deeper than 50 mbsf (Fig. 3A). Although scatter exists in the data, the ability of the model to fit the deeper sediments suggests that the shallow and deep sediments exhibit similar consolidation behavior. Yun et al. (2006) performed a consolidation model regression over the entire interval drilled at AT13-2 to define C_c equal to 0.292. The similarity of both C_c values also supports consistent consolidation behavior of all sediment at AT13-2.

AT13-2, ATM1, and ATM2 have similar water contents and void ratios that change relatively little from the seafloor to 27 mbsf (Fig. 2, Table 1). The similarity of shallow sub-bottom properties between mound and off-mound sediments is interesting because the sediment at the two locations is thought to have originated from different processes and been subject to different external stresses, namely fluidized transport from depth at the mound, in contrast to downslope mass wasting for the off-mound sediment. Similarity between properties above 4 mbsf may be explained by electro-chemical effects that can dominate deformation at shallow depths and prevent normal, mechanical consolidation (Francisca et al., 2005). With increasing depth, these electro-chemical effects are overwhelmed by increased effective stress. Yao and Anandarajah (2003) discuss the complexities and interactions of electro-chemcial effects, effective stress, and pore fluid composition on consolidation. The void ratio and water content trends at the mound could also result from these sediments having been buried more deeply and migrated to shallow depth; thus they have experienced higher effective stresses and have been unloaded but are recording the properties from deeper burial. This scenario could result from fluidized mud being transported from depth to the surface of the mound. Expulsion of mud from this mound is documented by seafloor imagery and bottom photography (Hart et al., 2008).

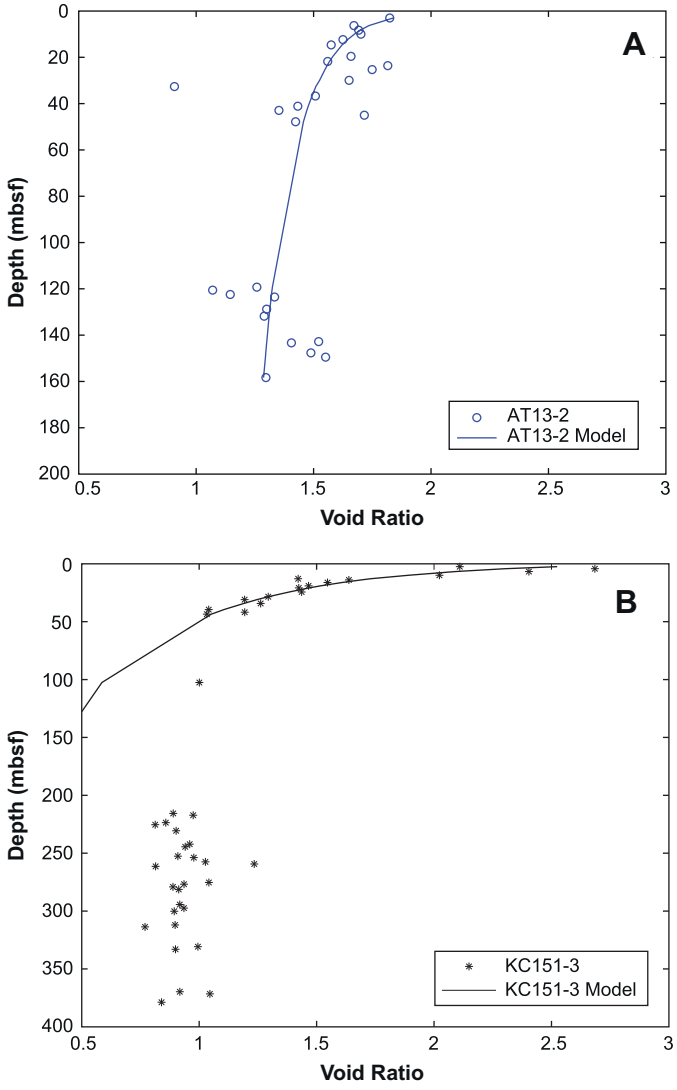

Fig. 3. (A) Measured (open circles) and modeled (solid line) void ratio for AT13-2. Void ratio model is based on a regression of the observations above 50 mbsf. (B) Measured (stars) and modeled (solid line) void ratio for KC151-3. Void ratio model is based on a regression of the observations above 50 mbsf. A change in deformation behavior below 50 mbsf is illuminated by the misfit of the void ratio model with the observations at depth.

Off-mound sediment, could achieve similar properties due to mass wasting that is prevalent in this area. Erosion causes unloading, which yields an overconsolidated state for the sediment that has been unloaded. Also, shear consolidation during remobilization can increase the consolidation state of sediment involved in mass wasting events (e.g., mass transport complexes) (Wood, 1990).

Keathley Canyon has a higher compression index (1.1) and reference void ratio (3.77) than AT13-2. The shallowly constrained consolidation model (<50 mbsf), however, does not reflect the consolidation behavior of the deeper sediments at KC151-3 (Fig. 3B). Deeper than 100 mbsf, measured void ratio is larger than predicted by the shallow-data model (Fig. 3B). Yun et al. (2006) also noted a change in shear strength below 50 mbsf, with sediments below 50 mbsf exhibiting reduced strength. Coring disturbance could also reduce shear strength (Yun et al., 2006), but this disturbance would have little effect on the bulk properties reported here because our sample selection targeted relatively intact core sections.

Although grain size is consistent from shallow to deep sediments (Table 2), composition and age may create differences in physical properties. The sediments below 200 mbsf have different resistivity than the shallow sediments (Collett, 2006), which could reflect mineralogic, bulk property, and porewater variations. This change in consolidation behavior is also located below an unconformity (Hutchinson et al., 2008). Time could facilitate chemical diagenesis or cementation that alters the consolidation behavior of sediments at depth. These lithologic and time changes with depth explain the discrepancy of our shallowly constrained C_c and the average C_c constrained by Yun et al. (2006) over the entire depth of the borehole.

An important aspect of our physical property measurements is validation of the well logging measurements. LWD measurements include the Azimuthal density neutron (ADN) tool which provided bulk density values (IDRO) every 0.1524 m at AT13-1 and KC151-2. Good agreement exists between the MAD bulk density (ρ_b) and the LWD bulk density (IDRO) (Fig. 4). With the exception of one MAD sample, the data at AT13-2 and AT13-1 (spaced ~12 m apart) overlie each other (Fig. 4A). In Keathley Canyon, ρ_b and IDRO data from wells with a 14 m horizontal offset overlie each other to 100 mbsf (Fig. 4B). Below 100 mbsf, the MAD data equal the minimum IDRO measurements. The overall agreement between the MAD and LWD bulk density measurements supports using LWD data (Lee and Collett, 2008) to understand sediment properties without additional core samples and analyses.

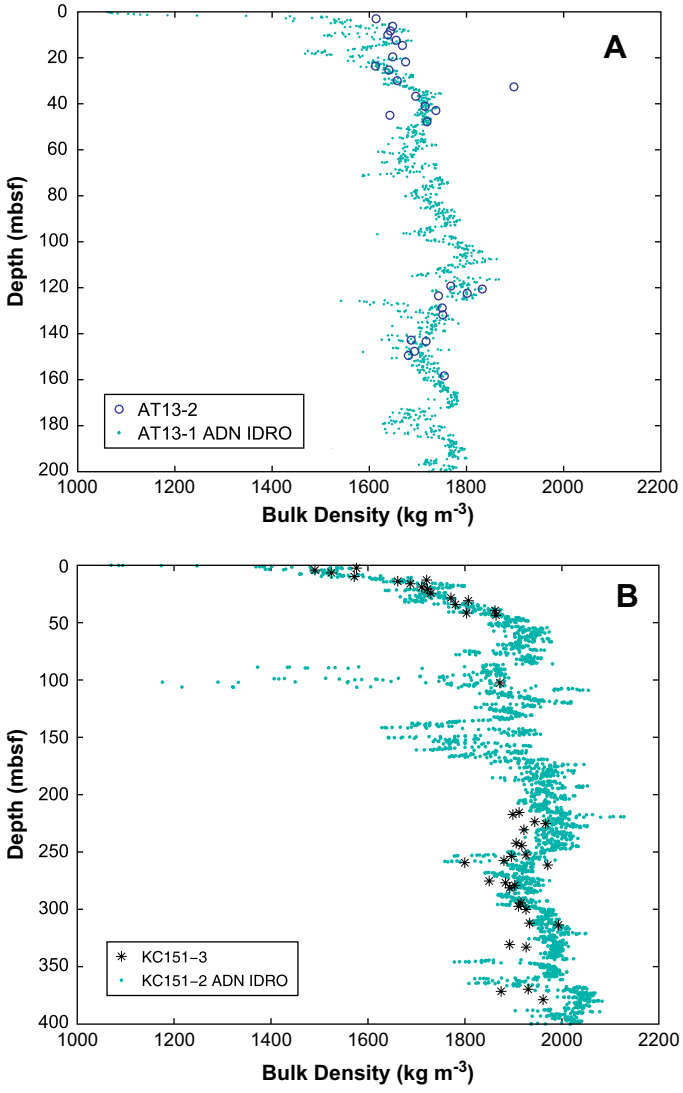

Fig. 4. (A) Bulk density from MAD analysis (open circles) and logging-while-drilling (dots) for twinned holes AT13-2 and AT13-1. MAD bulk density values are consistent with LWD measurements, which provide complete downhole coverage. LWD image-derived bulk density values (IDRO) were obtained from the Azimuthal density neutron (ADN) tool. (B) Bulk density from MAD analysis (stars) and logging-while-drilling (dots) for twinned holes KC151-3 and KC151-2. MAD bulk density values are consistent with LWD measurements.

Grain density ranges from 2670 to 2750 kg m^{-3} (Table 1), with mean and median values from 2690 to 2720 kg m^{-3}. These values are typical for fine-grained marine sediment (Keller, 1974). The sediments from Keathley Canyon have slightly higher grain density than those at Atwater Valley. The differences in grain density could reflect a different mineralogical content between the basins, different sediment sources, or different distances from the sediment source.

Carbon, hydrogen, and nitrogen concentrations were determined on 18 sediment samples from Atwater Valley and Keathley Canyon (Table 3). These elements represent between 0.05% and 2.65% of the total sample dry mass. Inorganic carbon (IC) (assumed to be bulk carbonate) ranged from 0.53% to 2.65%. Organic carbon (OC) ranged from 0.44% to 0.95%. This organic carbon range is between that of deep-sea (~0.15–0.20%) and near-shore (~1%) sediments (Chester, 2003). Organic carbon-to-total nitrogen (OC/TN) ratios vary from 7.44 to 9.29 at AT13-2, 9.50–10.17 at ATM1, and 8.80–16.40 at Keathley Canyon. The OC/TN ratios of organic matter from Atwater Valley sediment are consistent with a marine origin (7–10), whereas the OC/TN ratios for organic matter from Keathley Canyon are higher, which suggests a partially terrigenous organic contribution (>20) (Deevy, 1973; Rojas and Silva, 2005; Rullkotter, 2000). Interpretation of the difference in ratios between the three study areas suggests different origins of some sediment components, although it is recognized that diagenetic transformations, accumulation of microbial biomass, and adsorption of ammonium to clay particles may have altered the original source signature (Meyers, 1997).

Coulter Counter grain size analyses of Atwater Valley and Keathley Canyon sediments show that all sites are dominated by silty clay to clay-sized particles (Table 2). Although the extrapolation of grain-size results to a smaller size (Poppe et al., 2004) affects all calculated parameters, including D_{50} and C_u, we believe this extrapolation better characterizes the in situ sediment. Median (D_{50}) values vary from 1.0 to 2.8 μm with one outlier (Table 2). Although data extrapolation imparts some uncertainty, the grain-size results derived from this study are similar to average particle sizes for illite (0.1–2.0 μm diameter or length; Santamarina et al., 2001), the dominant clay mineral suggested by interpretation of specific surface measurements on other JIP samples from these cores (Yun et al., 2006) or from a location 24 km north in the Mississippi Canyon (Francisca et al., 2005). Furthermore, results from grain-size tests performed using the hydrometer method (Lambe, 1951; Fugro-McClelland Marine Geosciences, Inc., 2006) support our grain size measurements. At AT13-2, the average D_{50} values determined with a hydrometer agree exactly with the average D_{50} with a Coulter Counter. At KC151-3 the average D_{50} hydrometer value is 0.4 μm smaller than the average D_{50} Coulter Counter value.

The largest median grain size (6.91 μm) occurs at 102 mbsf in KC151-3 (Table 2), consistent with a quartz-rich horizon interpreted from logging operations (Collett, 2006). Using the extrapolation procedure described above, all samples have a C_u greater than 2.0 (Table 2), indicative of non-uniform, well-graded (poorly-sorted) sediment (Lambe and Whitman, 1969). Except for three samples from KC151-3, all skewness values are negative, meaning that cumulative grain-size distributions have an excess of coarse-grained particles relative to a normal distribution. Frequency curves

have higher kurtosis values and are therefore more peaked for sediment from Atwater Valley than from Keathley Canyon. This reflects an environment with a slightly higher sorting energy at Atwater Valley. The fine-grained nature of the sediment is consistent with a deepwater setting even though the depositional environments differ between these locations and may be locally complex (Hutchinson et al., 2008).

The possible presence of gas hydrate between 220 mbsf and 300 mbsf at KC151-3 does not appear to correlate with grain-size trends, unlike other geologic environments containing gas hydrate (Baba and Yamada, 2004; Dallimore and Collett, 2005; Fujii et al., 2005). However, a greater range in grain density values that may result from variations in sediment type is present in this interval. This potentially could influence fracture occurrence. Fractures in this interval have been interpreted to control the distribution of gas hydrate in Keathley Canyon (Collett, 2006; Hutchinson et al., 2008).

5. Conclusions

Physical properties measured in Atwater Valley and Keathley Canyon demonstrate similar grain density and grain size between the sites; however, their consolidation behavior differs. These deepwater (1300 m water depth) sites are dominated by silty clay-sized and clay-sized sediment with 1–3 μm median grain size. Although the grain-size properties are uniform, which overall might reflect either similar sources or distances from sources of the sediment, their depositional environments are different and the organic components of the sediments probably have different origins.

Consolidation profiles differ dramatically between the basins. Atwater Valley exhibits less physical property variation in the upper 27 mbsf compared to Keathley Canyon. The uniformity of bulk physical properties at the mound sites ATM1 and ATM2 may reflect sediments being expelled from depth. A consolidation model, based on shallow sediments at AT13-2, accurately predicts behavior to 200 mbsf. In contrast, shallow behavior at KC151-3 cannot predict behavior at depth because KC151-3 has two separate consolidation trends. The Keathley Canyon sediments above 50 mbsf follow a void ratio–effective vertical stress model but have higher compressibility than the Atwater Valley sediments. The sediments below 50 mbsf at Keathley Canyon consolidate differently than the shallow sediments. Diagenesis of the deeper sediments, facilitated by time and temperature, could yield a different consolidation trend.

The laboratory-based physical property measurements agree with the logging interpretations. The consistency between MAD and LWD bulk density measurements increases confidence in log-based interpretations and modeling at all sites.

Acknowledgments

The captain and crew of the Multi-Service Vessel Uncle John and Fugro-McClelland Marine Geosciences, Inc. are thanked for shipboard activities. L. Gilbert, E. Beaulieu, R. Wilcox-Cline, K. McMullen, and A. Green assisted with laboratory testing and data compilation. Support of this research was provided by the USGS Coastal and Marine Geology Program, the USGS Energy Program, and the National Energy Technology Laboratory. This manuscript benefited from constructive reviews by H. J. Lee, W. Bryant, E. Tripsanas, J. Pohlman, and an anonymous reviewer.

References

American Society for Testing and Materials, 1997. Standard test method for specific gravity of solids by gas pycnometer D5550-94. In: Soil and Rock. Annual Book of ASTM Standards, vol. 04.09. American Society for Testing and Materials, West Conshohocken, Pennsylvania, pp. 380–383.

American Society for Testing and Materials, 2006. Standard test methods for laboratory determination of water (moisture) content of soil and rock by mass D2216-05. In: Soil and Rock. Annual Book of ASTM Standards, vol. 04.08. American Society for Testing and Materials, West Conshohocken, Pennsylvania, pp. 205–211.

Baba, K., Yamada, Y., 2004. BSRs and associated reflections as an indicator of gas hydrate and free gas accumulation: an example of accretionary prism and forearc basin system along the Nankai Trough, off central Japan. Resour. Geol. 54 (1), 11–24.

Bird, D.E., Burke, K., Hall, S.A., Casey, J.F., 2005. Gulf of Mexico tectonic history; hotspot tracks, crustal boundaries, and early salt distribution. AAPG Bull. 89 (3), 311–328.

Blum, P., 1997. Physical Properties Handbook: A Guide to the Shipboard Measurement of Physical Properties of Deep-sea Cores. ODP Technical Note 26 Available from:. http://www-odp.tamu.edu/publications/tnotes/tn26/INDEX.HTM (accessed 11.05.07.).

Boggs Jr., S., 1992. Petrology of Sedimentary Rocks. Macmillan Publishing Company, New York, 707 pp.

Booth, J.S., Dahl, A.G., 1986. A note on the relationships between organic matter and some geotechnical properties of a marine sediment. Mar. Geotechnol. 6, 281–298.

Bowles, J.E., 1979. Physical and Geotechnical Properties of Soils. McGraw-Hill Book Co., New York, 478 pp.

Brydon, D., Sun, S., Bleck, R., 1999. A new approximation of the equation of state for seawater, suitable for numerical ocean models. J. Geophys. Res. 104, 1537–1540.

Cerato, A.B., Lutenegger, A.J., 2004. Determining intrinsic compressibility of fine-grained soils. J. Geotech. Geoenv. Eng. 130, 872–877.

Chester, R., 2003. Marine Geochemistry. Blackwell Publishing, Malden, Massachusetts, 506 pp.

Claypool, G.E., 2006. Gulf of Mexico Gas Hydrate Joint Industry Project (GOMJIP), 2005. The Cruise of the Drilling Vessel Uncle John, Mobile, Alabama to Galveston, Texas, Atwater Valley Blocks 13/14 and Keathley Canyon Block 151, 17 April to 22 May 2005 Available from: http://www.netl.doe.gov/technologies/oil-gas/publications/Hydrates/reports/GOMJIPCruise05.pdf.

Coffin, R.B., Hamdan, L., Plummer, R., Smith, J., Gardner, J., Hagen, R., Wood, W., 2008. Analysis of methane and sulfate flux in methane-charged sediments from the Mississippi Canyon, Gulf of Mexico. Mar. Petr. Geol. 25, 860–872.

Coleman, J., Prior, D., 1978. Submarine landslides in the Mississippi River delta. In: Offshore Technology Conference (OTC), pp. 1065–1074.

Coleman, J.M., Prior, D.B., Lindsay, J.F., 1983. Deltaic influences on shelf edge instability processes. In: Stanley, D.J., Moore, G.T. (Eds.), The Shelfbreak: Critical Interface on Continental Margins. SEPM, pp. 121–137.

Collett, T.S., 2006. Gulf of Mexico gas hydrate JIP drilling program downhole logging program, The Gulf of Mexico Gas Hydrate Joint Industry Project Cruise Report. National Energy Technology Laboratory. <http://www.netl.doe.gov/technologies/oil-gas/FutureSupply/MethaneHydrates/rd-program/GOM_JIP/hydrates_main.html, Morgantown, WV>

Cooper, A.K., Hart, P.E., 2003. High-resolution seismic-reflection investigation of the northern Gulf of Mexico gas-hydrate-stability zone. Mar. Petr. Geol. 19, 1275–1293.

Couper, A., 1983. The Times Atlas of the Oceans. Van Nostrand Reinhold Company, New York, 272 pp.

Dallimore, S.R., Collett, T.S., 2005. Summary and implications of the Mallik 2002 gas hydrate production research well program. In: Dallimore, S.R., Collett, T.S. (Eds.), Scientific Results from the Mallik 2002 Gas Hydrate Production Research Well Program, Mackenzie Delta, Northwest Territories, Canada. Geological Survey of Canada, Ottawa, pp. 1–36.

Deevy, E., 1973. Sulfur, nitrogen and carbon in the biosphere. In: Woodwell, G.M., Peacan, E.V. (Eds.), Carbon and the Biosphere. USAEC, Washington, D.C., pp. 182–190.

Fang, H.-Y., 1997. Introduction to Environmental Geotechnology. CRC Press, New York, 652 pp.

Flemings, P.B., Lupa, J., 2004. Pressure prediction in the Bullwinkle Basin through petrophysics and flow modeling (Green Canyon 65, Gulf of Mexico). Mar. Petr. Geol. 21, 1311–1322.

Flemings, P.B., Behrmann, J.H., John, C.M., Leg 308 Scientists, 2006. Proc. IODP 308, doi:10.2204/iodp.proc.308.2006 Integrated Ocean Drilling Program, College Station TX.

Francisca, F., Yun, T.-S., Ruppel, C., Santamarina, J.C., 2005. Geophysical and geotechnical properties of near-seafloor sediments in the northern Gulf of Mexico gas hydrate province. Earth Planet. Sci. Lett. 237, 924–939.

Fugro-McClelland Marine Geosciences, Inc, 2006. Geotechnical Investigation, Chevron Gulf of Mexico Gas Hydrates JIP, Blocks 13 and 14, Atwater Valley Area, Block 151, Keathley Canyon Area, Gulf of Mexico. Results of Core Sample Analysis, Standard and Advanced Laboratory Testing. Report 0201-5081. Fugro-McClelland Marine Geosciences, Inc., Houston, TX. Available from:. http://www.netl.doe.gov/technologies/oil-gas/FutureSupply/MethaneHydrates/rd-program/GOM_JIP/hydrates_main.html Morgantown, WV.

Fujii, T., Kawasaki, M., Nakamizu, M., Namikawa, T., Ochiai, K., Okui, T., Tsuji, Y., 2005. Modes of occurrence and accumulation mechanism of methane hydrate – result of METI exploratory test wells "Tokai-oki to Kumano-nada". In: Fifth International Conference on Gas Hydrates, Trondheim, Norway, pp. 974–979.

Goodwin, R.H., Prior, D.B., 1989. Geometry and depositional sequences of the Mississippi Canyon, Gulf of Mexico. J. Sediment. Petr. 59, 318–329.
Hart, P.E., Hutchinson, D.R., Gardner, J., Carney, R.S., Fornari, D., 2008. A photographic and acoustic transect across two deep-water seafloor mounds, Mississippi Canyon, northern Gulf of Mexico. Mar. Petr. Geol. 25, 969–976.
Harrison, W.J., Summa, L.L., 1991. Paleohydrology of the Gulf of Mexico basin. Am. J. Sci. 291, 109–176.
Holtz, R.D., Kovacs, W.D., 1981. An Introduction to Geotechnical Engineering. Prentice-Hall, Inc., Englewood Cliffs, New Jersey, 733 pp.
Hutchinson, D.R., Hart, P.E., Collett, T.S., Edwards, K.M., Twichell, D.C., Snyder, F., 2008. Geologic framework of the 2005 Keathley Canyon gas hydrate research well, northern Gulf of Mexico. Mar. Petr. Geol. 25, 906–918.
Jablonski, S.A., Mecray, E.L., Munson, J.M., Blackwood, D.S., 2002. Geochemical Sediment Analysis Procedures. Available from: http://pubs.usgs.gov/of/2002/of02-371/ Open-File Report 02–371, U.S. Geological Survey.
Kastner, M., Claypool, G., Robertson, G., 2006. Pore Water Geochemistry – 2005 Gulf of Mexico JIP Cruise, The Gulf of Mexico Gas Hydrate Joint Industry Project Cruise Report. National Energy Technology Laboratory, Morgantown, WV, pp. 1–14.
Kastner, M., Claypool, G.E., Robertson, G., 2008. Geochemical constraints on the origin of the pore fluids and gas hydrate distribution at Atwater Valley and Keathley Canyon, northern Gulf of Mexico. Mar. Petr. Geol. 25, 860–872.
Keller, G., 1974. Marine geotechnical properties: interrelationships and relationships to depth of burial. In: Inderbitzen, A. (Ed.), Deep Sea Sediments. Plenum Publishing Corporation, New York, pp. 77–100.
Kohl, B., Roberts, H.H., 1995. Mud volcanoes in the Gulf of Mexico: a mechanism for mixing sediments of different ages in slope environments. Gulf Coast Assoc. Geol. Soc. Trans. 45, 351–359.
Lambe, T.W., 1951. Soil Testing for Engineers. John Wiley & Sons, Inc., New York, 165 pp.
Lambe, T.W., Whitman, R.V., 1969. Soil Mechanics. John Wiley & Sons, New York, 553 pp.
Lee, M.W., Collett, T.S., 2008. Integrated analysis of well logs and seismic data at the Keathley Canyon, Gulf of Mexico, for estimation of gas hydrate concentrations. Mar. Petr. Geol. 25, 924–931.
Locat, J., Lee, H.J., Nelson, C.H., Schwab, W.C., Twichell, D.C., 1996. Analysis of the mobility of far reaching debris flows on the Mississippi Fan, Gulf of Mexico. In: Senneset, K. (Ed.), Proceedings of the Seventh Internaional Symposium on Landslides. A.A. Balkema, Rotterdam, Trondheim, Norway, pp. 555–560.
MacDonald, I.R., Leifer, I., Sassen, R., Stine, P., Mitchell, R., Guinasso Jr., N., 2002. Transfer of hydrocarbons from natural seeps to the water column and atmosphere. Geofluids 2, 95–107.
Meyers, P.A., 1997. Organic geochemical proxies of paleoceanographic, paleolimnologic, and paleoclimatic processes. Org. Geochem. 27, 213–250.
Mitchell, J.K., 1976. Fundamentals of Soil Behavior. John Wiley & Sons, Inc., New York, 422 pp.
Ostermeier, R.M., Pelletier, J.H., Winker, C.D., Nicholson, J.W., Rambow, F.H., Cowan, K.M., 2000. Dealing with shallow-water flow in the deepwater Gulf of Mexico. Offshore Technology Conference Paper #11972.
Poppe, L.J., Elisaon, A.H., Hastings, M.E., 2004. A Visual Basic program to generate grain-size statistics and to extrapolate particle distributions. Comp. Geosci. 30, 791–795.
Poppe, L.J., Williams, S.J., Paskevich, V.F., 2005. U.S. Geological Survey East-Coast Sediment Analysis: Procedures, Database, and GIS Data. U.S. Geological Survey Open-File Report 2005-1001 Available from:. http://pubs.usgs.gov/of/2005/1001/.
Prior, D.B., Coleman, J.M., 1984. Submarine slope instability. In: Brunsden, D., Prior, D.B. (Eds.), Slope Instability. John Wiley & Sons, New York, pp. 419–455.
Rojas, N., Silva, N., 2005. Early diagenesis and vertical distribution of organic carbon and total nitrogen in recent sediments from southern Chilean fjords (Boca del Guafo to Pulluche Channel). Invest. Mar. Valparaiso 33 (2), 183–194.
Roberts, H.H., 2001. Fluid and gas expulsion on the northern Gulf of Mexico continental slope: mud-prone to mineral-prone responses. In: Paull, C.K., Dillon, W. (Eds.), Natural Gas Hydrates: Occurrence, Distribution and Detection. American Geophysical Union Monograph, vol. 124. AGA, Washington, D.C., pp. 145–161.
Rullkotter, J., 2000. Organic matter: the driving force for early diagenesis. In: Schulz, H.D., Zabel, M. (Eds.), Marine Geochemistry. Springer-Verlag, Berlin, pp. 129–172.
Ruppel, C., Dickens, G.R., Castellini, D.G., Gilhooly, W., Lizarralde, D., 2005. Heat and salt inhibition of gas hydrate formation in the northern Gulf of Mexico. Geophys. Res. Lett. 32, L04605, doi:10.1029/2004GL021909.
Sager, W.W., MacDonald, I.R., Hou, R., 2003. Geophysical signatures of mud mounds at hydrocarbon seeps on the Louisianna continental slope, northern Gulf of Mexico. Mar. Geol. 198, 97–132.
Salvador, A., 1991. The Gulf of Mexico Basin, The Geology of North America. Geological Society of America, Boulder, CO, 568 pp.
Santamarina, J.C., Klein, K.A., Fam, M.A., 2001. Soils and Waves. John Wiley & Sons, Chichester, England, 488 pp.
Seldon, B., Flemings, P.B., 2005. Reservoir pressure and seafloor venting: predicting trap integrity in a deepwater turbidite reservoir. AAPG Bull. 89, 193–209.
Shepard, F.P., 1954. Nomenclature based on sand-silt-clay ratios. J. Sediment. Petr. 24, 151–158.
Syvitski, J.P.M., 1991. Principles, Methods, and Application of Particle Size Analysis. Cambridge University Press, Cambridge, 368 pp.
Verardo, D.J., Froelich, P.N., McIntyre, A., 1990. Determination of organic carbon and nitrogen in marine sediments using the Carlo Erba NA-1500 analyzer. Deep Sea Res. Oceanogr. Res. Paper 37, 157–165.
Wentworth, C.K., 1929. Method of computing mechanical composition of sediments. Geol. Soc. Am. Bull. 40, 771–790.
Winker, C.D., Booth, J.R., 2000. Sedimentary dynamics of the salt-dominated continental slope, Gulf of Mexico: integration of observations from the seafloor, near-surface, and deep subsurface. In: Weimer, P.S., Slatt, R.M., Coleman, J., Rosen, N.C., Nelson, H., Bouma, A.H., Styzen, M.J., Lawrence, D.T. (Eds.), Deep-Water Reservoirs of the World: Proceedings of the Gulf Coast Section SEPM, pp. 1059–1086.
Winters, W.J., 2000. Data report; effects of drying methods and temperatures on water content and porosity of sediment from the Blake Ridge. In: Paull, C.K., Matsumoto, R., Wallace, P.J., Dillon, W.P. (Eds.), Proceedings of the Ocean Drilling Program, Scientific Results, vol. 164, pp. 431–434.
Wood, D.M., 1990. Soil Behavior and Critical State Soil Mechanics. Cambridge University Press, Cambridge, 462 pp.
Wood, W.T., Hart, P.E., Hutchinson, D.R., Dutta, N., Snyder, F., Coffin, R.B., Gettrust, J.F., 2008. Gas and gas hydrate distribution around seafloor seeps in Mississippi Canyon, Northern Gulf of Mexico, using multi-resolution seismic imagery. Mar. Petr. Geol. 25, 952–959.
Worrall, D.M., Snelson, S., 1989. Evolution of the northern Gulf of Mexico, with emphasis on Cenozoic growth faulting and the role of salt. In: Bally, A.W., Paler, A.R. (Eds.), The Geology of North America – An Overview, vol. A. Geological Society of America, Boulder, CO, pp. 97–137.
Wright, D.G., 1997. An equation of state for use in ocean models: Eckart's formula revisited. J. Atmos. Ocean. Technol. 14, 735–740.
Yao, M., Anandarajah, A., 2003. Three-dimensional discrete element method of analysis of clays. J. Eng. Mech. 129 (6), 585–596, doi:10.1061/(ASCE)0733-93992003129.
Yun, T.S., Narsilio, G.A., Santamarina, J.C., 2006. Physical characterization of core samples recovered from Gulf of Mexico. Mar. Petr. Geol. 23, 893–900.